

LETTER TO THE EDITOR

Threshold velocity for collisional growth of porous dust aggregates consisting of cohesive frictionless spheres

Sota Arakawa¹, Hidekazu Tanaka², Eiichiro Kokubo³, Daisuke Nishiura¹, and Mikito Furuichi¹

¹ Japan Agency for Marine-Earth Science and Technology, 3173-25, Showa-machi, Kanazawa-ku, Yokohama, 236-0001, Japan
e-mail: arakawas@jamstec.go.jp

² Astronomical Institute, Graduate School of Science, Tohoku University, 6-3 Aramaki, Aoba-ku, Sendai, 980-8578, Japan

³ National Astronomical Observatory of Japan, 2-21-1, Osawa, Mitaka, Tokyo, 181-8588, Japan

Received DD/MM/YYYY; accepted DD/MM/YYYY

ABSTRACT

Understanding the collisional outcomes of dust aggregates and dependence on material properties of the constituting particles is of great importance toward understanding planet formation. Recent numerical simulations have revealed that interparticle tangential friction plays a crucial role in energy dissipation during collisions between porous dust aggregates; however, the importance of friction on the collisional growth of dust aggregates remains poorly understood. Here we demonstrate the effects of interparticle tangential friction on the collisional growth of dust aggregates. We performed numerical simulations of collisions between equal-mass porous dust aggregates consisting of cohesive and frictionless spheres. We changed the collision velocity and impact angle systematically and calculated the collisional growth efficiency as a function of the collision velocity. We found that the threshold velocity for collisional growth decreases when dust aggregates are made of frictionless spheres as compared to frictional spheres. Our results highlight the importance of tangential interactions on the collisional behavior of dust aggregates and indicate that the predictive equation for threshold velocity should be reconstructed.

Key words. Planets and satellites: formation – Protoplanetary disks

1. Introduction

Collisional growth of dust aggregates consisting of micro/nanosized grains is ubiquitous in the universe. For example, collisional growth of soot nanoparticles produced by combustion processes is important in environmental science and engineering (e.g., Haynes & Wagner 1981). Atmospheric hazes on the early Earth and other planetary bodies are also dust aggregates consisting of micro/nanosized particles, and their collisional growth affects the atmospheric structure (e.g., Trainer et al. 2006; Zhang et al. 2017; Ohno et al. 2021). The first step of planet formation in circumstellar disks is collisional growth of micro/nanosized interstellar dust particles (e.g., Hayashi et al. 1985; Drazkowska et al. 2022), and dust growth might also trigger the formation of planetary objects around supermassive black holes in a galactic center (e.g., Wada et al. 2021).

The condition for collisional growth of dust aggregates has been studied both by laboratory experiments (e.g., Blum & Wurm 2008; Güttler et al. 2010; Fritscher & Teiser 2021; Schräpler et al. 2022) and numerical simulations (e.g., Wada et al. 2009; Seizinger et al. 2013; Hasegawa et al. 2021; Osinsky & Brilliantov 2022). These previous studies found that the growth/fragmentation conditions depend on the strength of interparticle forces acting on constituent particles in contact with each other.

Wada et al. (2009) performed a large number of numerical simulations of collisions between two equal-mass dust aggregates consisting of submicron-sized spherical ice particles. They varied the collision velocities and impact angles and obtained the collisional growth efficiency. Their numerical simulations revealed that the threshold velocity for collisional

growth/fragmentation of dust aggregates, v_{fra} , is approximately 60 m s^{-1} when the radius of constituting particles is $0.1 \mu\text{m}$ and the initial aggregates before collisions are prepared by ballistic particle-cluster aggregation (BPCA; Mukai et al. 1992). They also predicted that v_{fra} would be proportional to the square root of the energy required for breaking one interparticle contact, E_{break} , which is related to the connection/disconnection of particles due to interparticle normal motion (e.g., Dominik & Tielens 1997; Wada et al. 2007).

Arakawa et al. (2022b) also performed numerical simulations of collisions between dust aggregates and investigated the dependence of the threshold velocity on the strength of the viscous dissipation. They found that the main energy dissipation mechanism is not the normal interaction (i.e., viscous dissipation and connection/disconnection of particles) but the rolling friction between particles in contact.

Then Arakawa et al. (2022a) investigated the dependence of the threshold velocity on the strength of rolling friction. They revealed that the threshold velocity barely depends on the strength of rolling friction, however. In their simulations, frictions arising from two other tangential motions (sliding and twisting) complemented the change in energy dissipation due to rolling friction.

Energy dissipation is essentially required for collisional growth of dust aggregates. The results of Arakawa et al. (2022b,a) indicate that the threshold velocity for collisional growth/fragmentation are affected by the presence/absence of interparticle tangential frictions when the motions cannot complement one another.

Here, we report numerical simulations of collisions between two equal-mass dust aggregates consisting of submicron-sized

spherical ice particles, with and without interparticle frictions. We also systematically varied the collision velocities and impact angles, and we calculated the collisional growth efficiency by averaging over impact angles. We confirmed that the collisional growth efficiency of dust aggregates clearly depends on the presence/absence of interparticle frictions associated with tangential motions. Our results indicate that the dependence of the collisional growth efficiency on the material properties of constituent particles are more complex than previously assumed.

2. Model

We performed three-dimensional numerical simulations of collisions between two equal-mass dust aggregates. Our numerical code was originally developed by Wada et al. (2007), and Arakawa et al. (2022b) introduced a viscous drag force for normal motion (e.g., Krijt et al. 2013). We prepared two initial aggregates before collisions by BPCA as in previous studies (Wada et al. 2009; Arakawa et al. 2022b,a). We set the number of particles in the target aggregate, N_{tar} , equal to that for the projectile aggregate, N_{pro} , and the total number of particles in a simulation, $N_{\text{tot}} = N_{\text{tar}} + N_{\text{pro}}$, is 100,000. The constituent dust particles are made of water ice and the particle radius is $r_1 = 0.1 \mu\text{m}$. The particle interaction model is briefly described in Appendix A.

The strength of interparticle normal dissipation is controlled by a parameter called the viscoelastic timescale, T_{vis} (e.g., Arakawa et al. 2022b). We performed numerical simulations with two models for interparticle normal dissipation: with dissipation ($T_{\text{vis}} = 6 \text{ ps}$) and without dissipation ($T_{\text{vis}} = 0 \text{ ps}$; see Appendix A.1).

The strengths of interparticle tangential frictions are characterized by the spring constants for rolling (k_r), sliding (k_s), and twisting (k_t). In this study, we also performed numerical simulations with two models for interparticle tangential motions: the frictional and frictionless models. In the frictional model, we consider the interparticle tangential interactions as modeled by Wada et al. (2007), and we used the same values of k_r , k_s , and k_t as assumed in Wada et al. (2007). In the frictionless model, in contrast, we do not consider the interparticle tangential frictions; in other words, we set $k_r = k_s = k_t = 0$ (see Appendix A.2).

3. Results

Figure 1 shows snapshots of the collisional outcomes. We show the numerical results for the frictionless model ($k_r = k_s = k_t = 0$) without normal dissipation ($T_{\text{vis}} = 0 \text{ ps}$), and we set $v_{\text{col}} = 39.8 \text{ m s}^{-1}$, where v_{col} is the collision velocity of two dust aggregates. We found that the collisional behavior strongly depends on the impact angles. Comparing Figure 1(c) with Figure 2 of Arakawa et al. (2022a), we can visually understand that the collisional behavior also depends on the interparticle interaction model. Arakawa et al. (2022a) presented the results for the same collision velocity and impact angle, but used the frictional model with normal dissipation. In contrast, Figure 1(c) of this study shows the results for the frictionless model without normal dissipation. We found that the amount of small fragments significantly increases as compared to the results of Arakawa et al. (2022a).

In this study, we use the normalized impact parameter, B_{off} , to quantify the offset of oblique collisions. We defined B_{off} as $B_{\text{off}} = b_{\text{off}}/b_{\text{max}}$, where b_{off} is the impact parameter and b_{max} is the sum of the radii of the target and projectile aggregates (see Arakawa et al. 2022b). The radius of dust aggregates is set equal

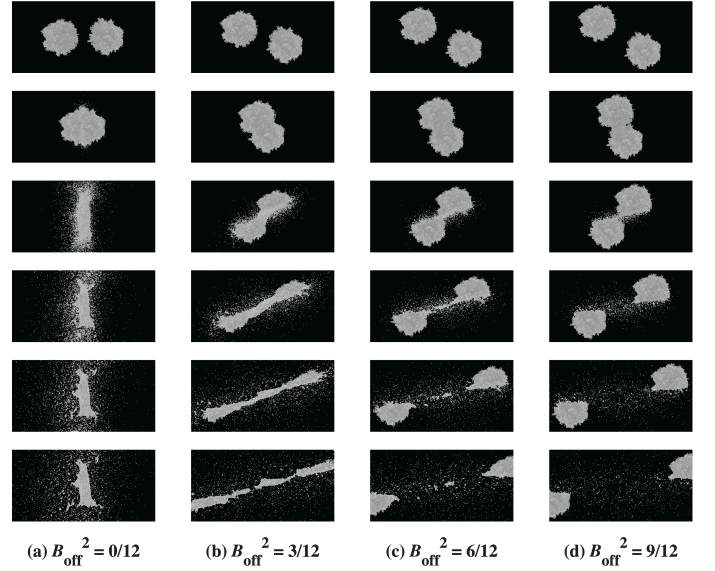


Fig. 1. Snapshots of the collisional outcomes. Here, we show the numerical results for the frictionless model ($k_r = k_s = k_t = 0$) without normal dissipation ($T_{\text{vis}} = 0 \text{ ps}$), and we set $v_{\text{col}} = 39.8 \text{ m s}^{-1}$. Panels (a)–(d) are the time series of snapshots for $B_{\text{off}}^2 = 0/12, 3/12, 6/12$, and $9/12$, respectively. The time interval for each snapshot is $0.40 \mu\text{s}$.

to the characteristic radius, r_c , which is given by $r_c = \sqrt{5/3} r_g$, where r_g is the gyration radius (e.g., Mukai et al. 1992; Wada et al. 2009). It is clear that $B_{\text{off}}^2 = 0$ for head-on collisions, and B_{off}^2 ranges from 0 to 1.

When considering collisions in space, the impact parameter should vary with each collision event. The average value of a variable A weighted over B_{off} ,

$$\langle A \rangle \equiv \int_0^1 dB_{\text{off}} 2B_{\text{off}} A, \quad (1)$$

is useful to measure the average outcome of the collision.

3.1. Collisional growth efficiency and the threshold velocity for collisional growth/fragmentation

Figure 2 shows the B_{off} -weighted collisional growth efficiency, $\langle f_{\text{gro}} \rangle$, as a function of v_{col} for different particle interaction models. The growth efficiency, f_{gro} , is defined for each simulation, and it is given by $f_{\text{gro}} = (N_{\text{lar}} - N_{\text{tar}})/N_{\text{pro}}$, where N_{lar} denotes the number of constituent particles in the largest remnant (see Hasegawa et al. 2021). The collisional outcome of each simulation is summarized in Figure B.1 (see Appendix B).

We found that $\langle f_{\text{gro}} \rangle$ clearly depends on the choice of particle interaction models. In our simulation of the frictional model without normal dissipation (gray solid line), $\langle f_{\text{gro}} \rangle \simeq 0$ at approximately $v_{\text{col}} = 60 \text{ m s}^{-1}$. Wada et al. (2009) also performed simulations with the same particle interaction model and their result is in excellent agreement with ours. Here we define the threshold velocity for collisional growth/fragmentation, v_{fra} , as the collision velocity that satisfies $\langle f_{\text{gro}} \rangle = 0$.

In the frictional model with normal dissipation (gray dashed line), we found that $v_{\text{fra}} \simeq 50 \text{ m s}^{-1}$, which is close to the value for the frictional model without normal dissipation. The dependence of $\langle f_{\text{gro}} \rangle$ on v_{col} in frictional models with and without normal dissipation is similar; their difference in $\langle f_{\text{gro}} \rangle$ is typically less than 0.1 in the range of $10 \text{ m s}^{-1} \leq v_{\text{col}} \leq 100 \text{ m s}^{-1}$.

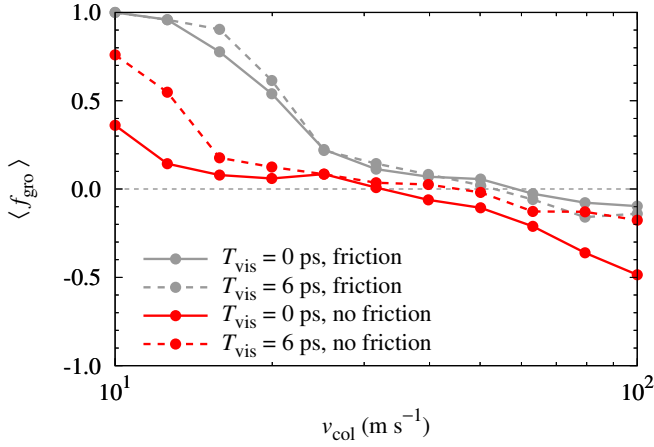


Fig. 2. B_{off} -weighted collisional growth efficiency, $\langle f_{\text{gro}} \rangle$. We note that the results for frictional models (gray lines) are identical to those presented in Figure 3 of Arakawa et al. (2022b) for $v_{\text{col}} \geq 20.0 \text{ m s}^{-1}$.

Arakawa et al. (2022b) concluded that this independence of $\langle f_{\text{gro}} \rangle$ on the presence/absence of normal dissipation is consistent with the fact that the main energy dissipation mechanism is not normal dissipation but interparticle tangential friction when using frictional models for particle interaction.

In frictionless models, however, we found that v_{fra} is significantly lower than that of frictional models, e.g., $v_{\text{fra}} \approx 30 \text{ m s}^{-1}$ in the frictionless model without normal dissipation (red solid line). In addition, $\langle f_{\text{gro}} \rangle$ also decreases compared to the frictional models. For example, $0.1 \lesssim \langle f_{\text{gro}} \rangle \lesssim 0.2$ at $v_{\text{col}} = 15.8 \text{ m s}^{-1}$ in frictionless models, while $0.8 \lesssim \langle f_{\text{gro}} \rangle \lesssim 0.9$ at the same v_{col} in frictional models. These differences would be related to the difference in energy dissipation processes (see Appendix C).

We note that v_{fra} depends on the presence/absence of normal dissipation when tangential frictions are absent. In the frictionless model with normal dissipation (red dashed line), our numerical results show that $v_{\text{fra}} \approx 45 \text{ m s}^{-1}$, which is 1.5 times larger than that of the frictionless model without normal dissipation. Figure 2 shows that $\langle f_{\text{gro}} \rangle$ for the frictionless model with normal dissipation is significantly higher than that of the frictionless model without normal dissipation in the ranges of $v_{\text{col}} \ll 20 \text{ m s}^{-1}$ and $v_{\text{col}} \gg 60 \text{ m s}^{-1}$, although their difference in $\langle f_{\text{gro}} \rangle$ is roughly within 0.1 in the intermediate range of v_{col} .

Based on the results of Wada et al. (2009), Wada et al. (2013) proposed an empirical formula to estimate v_{fra} as a function of the particle radius and material properties of constituting particles. The empirical formula is $v_{\text{fra}} \approx 15 \sqrt{E_{\text{break}}/m_1}$, where m_1 is the mass of each particle. As both E_{break} and m_1 are independent of the spring constants for tangential motions (k_t , k_s , and k_l), this equation cannot express the effects of tangential interactions on v_{fra} . Our numerical results, however, highlight the impact of tangential interactions on v_{fra} . Thus we need to modify the prediction formula for v_{fra} .

Our results indicate that v_{fra} depends not only on E_{break} but also on interparticle energies associated with tangential motions. It is important to note that their dependences on the particle radius and material properties are different from each other (see Wada et al. 2007). For example, E_{break} is proportional to $r_1^{4/3}$ (see Appendix A.1), while the energy needed to slide a particle by $\pi/2$ radian around its contact point, E_{slide} , is proportional to $r_1^{7/3}$. The energy needed to twist over $\pi/2$ radian, E_{twist} , is proportional to r_1^2 (see Appendix A.2). Although it seems an

extreme and unrealistic assumption, v_{fra} might be proportional to $r_1^{-1/3}$ when it is proportional to $\sqrt{E_{\text{slide}}/m_1}$, or v_{fra} might be proportional to $r_1^{-1/2}$ when it is proportional to $\sqrt{E_{\text{twist}}/m_1}$.

Blum & Wurm (2008) reviewed laboratory experiments of collisions of dust aggregates and reported that the threshold velocity for sticking of dust aggregates is proportional to r_1^{-x} , with $x \gtrsim 1$ for $0.1 \mu\text{m} \lesssim r_1 \lesssim 1 \mu\text{m}$ and $x \lesssim 1$ for $1 \mu\text{m} \lesssim r_1 \lesssim 10 \mu\text{m}$. Although these experimental results are for head-on collisions and it cannot be directly compared with our B_{off} -weighted numerical results, we can speculate that the dependence of v_{fra} on r_1 might not be given by a simple power-law relation.

3.2. Size distribution of fragments

As shown in Figure 1, collisions of dust aggregates consisting of frictionless particles without normal dissipation ($k_t = k_s = k_l = 0$ and $T_{\text{vis}} = 0 \text{ ps}$) produce a large amount of small fragments. In circumstellar disks, the strength of turbulence driven by magnetorotational instability is a function of the gas ionization degree and depends on the amount of small dust aggregates (e.g., Okuzumi & Hirose 2012). Thus, the amount of small dust aggregates might also be the key parameter for planet formation via collisional growth of dust aggregates. Here, we quantify the size distribution of fragments in our simulations (see also Arakawa et al. 2022b; Hasegawa et al. 2022; Osinsky & Brilliantov 2022).

Arakawa et al. (2022b) defined $N_{\text{cum}}(\leq N)$ as the cumulative number of particles that are constituents of fragments that contain not larger than N particles. Figure 3 shows the B_{off} -weighted average of $N_{\text{cum}}(\leq N)$, $\langle N_{\text{cum}}(\leq N) \rangle$. We found that $\langle N_{\text{cum}}(\leq N) \rangle$ significantly differs among particle interaction models.

As shown in Figure 3, the size distributions of fragments for frictional models with and without normal dissipations (gray dashed and solid lines, respectively) are similar, particularly for larger fragments ($N > 10$ for $v_{\text{col}} = 20.0 \text{ m s}^{-1}$ and $N > 10^3$ for $v_{\text{col}} = 39.8 \text{ m s}^{-1}$). This trend is consistent with the results of Arakawa et al. (2022b).

We found that the amount of small fragments strongly depends on the presence/absence of interparticle tangential friction. When we apply the frictionless model without normal dissipation for constituting particles (red solid line), the amount of small fragments with $N < 10^2$ was orders of magnitude larger than that of the frictional models. This difference might also imply the importance of interparticle tangential frictions on the energy dissipation and deformation of dust aggregates during collision.

We note that for frictionless models, the size distribution of fragments clearly depends on the strength of normal dissipation (T_{vis}). Considering $v_{\text{col}} = 20.0 \text{ m s}^{-1}$ as an example, the difference in $\langle f_{\text{gro}} \rangle$ is small (approximately 0.1; Figure 2), but the difference in $\langle N_{\text{cum}}(\leq N) \rangle$ is approximately two orders of magnitude for $N < 10^2$. These simulation results might indicate that the mechanisms for aggregate-wide deformation and the ejection of small fragments are different. We will test this hypothesis in future studies.

4. Conclusions

Understanding the collisional behavior of dust aggregates consisting of micro/nanosized grains is essential to understanding planet formation. The threshold velocity for collisional growth/fragmentation, v_{fra} , is one of the most important parameters that controls the size of dust aggregates in circumstellar disks (e.g., Okuzumi & Tazaki 2019; Arakawa et al. 2021); how-

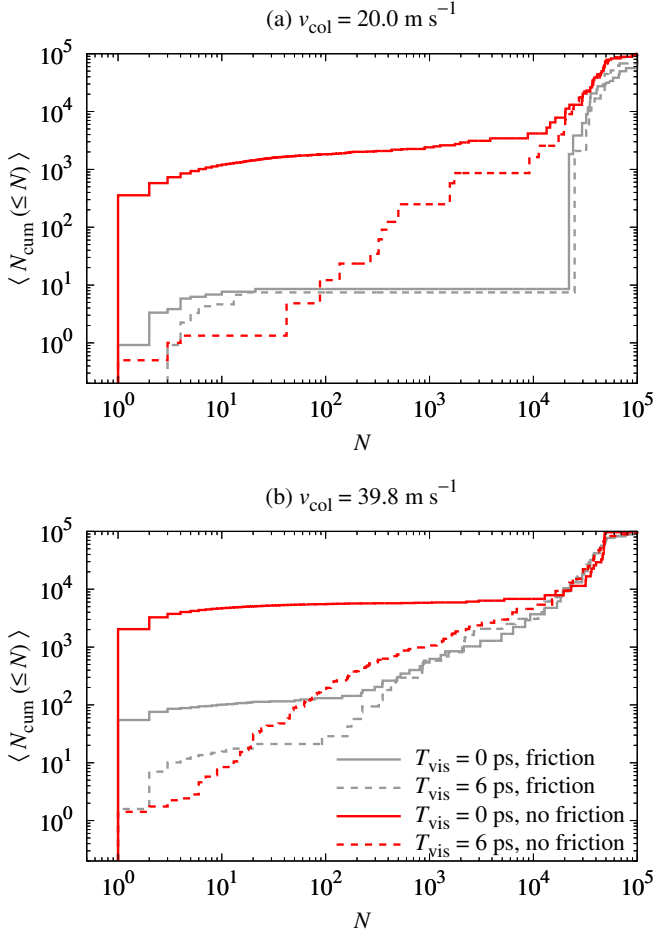


Fig. 3. B_{off} -weighted average of $N_{\text{cum}}(\leq N)$, $\langle N_{\text{cum}}(\leq N) \rangle$. (a) For the case of $v_{\text{col}} = 20.0 \text{ m s}^{-1}$. (c) For the case of $v_{\text{col}} = 39.8 \text{ m s}^{-1}$.

ever, the dependence of v_{fra} on the particle radius and the material properties of constituting particles is still under debate.

Arakawa et al. (2022b,a) revealed that the main energy dissipation mechanism for oblique collisions of dust aggregates is not the interparticle normal interaction (i.e., connection and disconnection of particles) but the tangential friction between particles in contact with each other. Thus, we expect that the collisional outcomes of dust aggregates could depend on the strength of interparticle frictions.

In this study, we demonstrated that v_{fra} depends on the strength of tangential interactions using numerical simulations of collisions between dust aggregates. We tested $2 \times 2 = 4$ types of particle interaction models in this study. In these models, the presence/absence of the interparticle tangential frictions is captured by differences in the spring constants (k_r , k_s , and k_t), and the presence/absence of the normal dissipation is captured by differences in the viscoelastic timescale (T_{vis}).

In the frictional model without normal dissipation, we found that $v_{\text{fra}} \simeq 60 \text{ m s}^{-1}$, which is consistent with that reported in previous studies (e.g., Wada et al. 2009; Hasegawa et al. 2021). In contrast, in the frictionless model without normal dissipation, we found that $v_{\text{fra}} \simeq 30 \text{ m s}^{-1}$, which is notably lower than that of the frictional model (see Figure 2). We also found that v_{fra} depends on the presence/absence of the normal dissipation when tangential frictions are absent, while v_{fra} is nearly independent of T_{vis} for frictional models. Our results further indicate that the dependence of v_{fra} on the particle radius and material properties

cannot be described by a simple power-law relation (see Blum & Wurm 2008; Wada et al. 2009, 2013). Future studies on this point are essential, although a large number of numerical simulations are needed to construct a better fitting formula to predict v_{fra} as a function of particle radius and material properties.

The size distribution of fragments also depends on the choice of particle interaction models (see Figure 3). As shown in Figure 1, collisions of dust aggregates consisting of frictionless particles without normal dissipation produce a large amount of small fragments. We also found that for frictionless models, the size distribution of fragments significantly depends on the strength of normal dissipation, even if the difference in $\langle f_{\text{gro}} \rangle$ is small. Our results might indicate that the mechanisms for aggregate-wide deformation and the ejection of small fragments are different, although we need to investigate this hypothesis in future studies.

Acknowledgements. The anonymous reviewer provided a constructive review that improved this paper. Numerical computations were carried out on PC cluster at CfCA, NAOJ. H.T. and E.K. were supported by JSPS KAKENHI grant No. 18H05438. We thank American Journal Experts (AJE) for English language editing.

References

- Arakawa, S. & Krijt, S. 2021, *ApJ*, 910, 130
- Arakawa, S., Matsumoto, Y., & Honda, M. 2021, *ApJ*, 920, 27
- Arakawa, S., Tanaka, H., & Kokubo, E. 2022a, *ApJ*, 939, 100
- Arakawa, S., Tanaka, H., & Kokubo, E. 2022b, *ApJ*, 933, 144
- Blum, J. & Wurm, G. 2008, *ARA&A*, 46, 21
- Dominik, C. & Tielens, A. G. G. M. 1995, *Philosophical Magazine, Part A*, 72, 783
- Dominik, C. & Tielens, A. G. G. M. 1996, *Philosophical Magazine, Part A*, 73, 1279
- Dominik, C. & Tielens, A. G. G. M. 1997, *ApJ*, 480, 647
- Draskowska, J., Bitsch, B., Lambrechts, M., et al. 2022, *arXiv e-prints*, arXiv:2203.09759
- Fritscher, M. & Teiser, J. 2021, *ApJ*, 923, 134
- Gundlach, B. & Blum, J. 2015, *ApJ*, 798, 34
- Güttler, C., Blum, J., Zsom, A., Ormel, C. W., & Dullemond, C. P. 2010, *A&A*, 513, A56
- Hasegawa, Y., Suzuki, T. K., Tanaka, H., Kobayashi, H., & Wada, K. 2021, *ApJ*, 915, 22
- Hasegawa, Y., Suzuki, T. K., Tanaka, H., Kobayashi, H., & Wada, K. 2022, *arXiv e-prints*, arXiv:2212.10796
- Hayashi, C., Nakazawa, K., & Nakagawa, Y. 1985, in *Protostars and Planets II*, ed. D. C. Black & M. S. Matthews, 1100–1153
- Haynes, B. S. & Wagner, H. G. 1981, *Progress in Energy and Combustion Science*, 7, 229
- Johnson, K. L., Kendall, K., & Roberts, A. D. 1971, *Proceedings of the Royal Society of London Series A*, 324, 301
- Krijt, S., Güttler, C., Heißelmann, D., Dominik, C., & Tielens, A. G. G. M. 2013, *Journal of Physics D Applied Physics*, 46, 435303
- Mukai, T., Ishimoto, H., Kozasa, T., Blum, J., & Greenberg, J. M. 1992, *A&A*, 262, 315
- Musiolik, G., Teiser, J., Jankowski, T., & Wurm, G. 2016, *ApJ*, 827, 63
- Ohno, K., Zhang, X., Tazaki, R., & Okuzumi, S. 2021, *ApJ*, 912, 37
- Okuzumi, S. & Hirose, S. 2012, *ApJ*, 753, L8
- Okuzumi, S. & Tazaki, R. 2019, *ApJ*, 878, 132
- Osinsky, A. & Brilliantov, N. 2022, *Physica A: Statistical Mechanics and its Applications*, 603, 127785
- Schräpler, R. R., Landeck, W. A., & Blum, J. 2022, *MNRAS*, 509, 5641
- Seizinger, A., Krijt, S., & Kley, W. 2013, *A&A*, 560, A45
- Trainer, M. G., Pavlov, A. A., Dewitt, H. L., et al. 2006, *Proceedings of the National Academy of Science*, 103, 18035
- Wada, K., Tanaka, H., Okuzumi, S., et al. 2013, *A&A*, 559, A62
- Wada, K., Tanaka, H., Suyama, T., Kimura, H., & Yamamoto, T. 2007, *ApJ*, 661, 320
- Wada, K., Tanaka, H., Suyama, T., Kimura, H., & Yamamoto, T. 2009, *ApJ*, 702, 1490
- Wada, K., Tsukamoto, Y., & Kokubo, E. 2021, *ApJ*, 909, 96
- Zhang, X., Strobel, D. F., & Imanaka, H. 2017, *Nature*, 551, 352

Appendix A: Particle interaction model

Here, we briefly explain the particle interaction model used in this study. Details are described in [Wada et al. \(2007\)](#) and [Arakawa et al. \(2022b\)](#).

Appendix A.1: Normal motion

We assume that the normal force acting between two particles, F , is given by the sum of the two terms:

$$F = F_E + F_D, \quad (\text{A.1})$$

where F_E denotes the force arising from the elastic deformation of particles and F_D is the force related to the viscous dissipation.

When two particles in contact are elastic spheres with a surface energy, the elastic term is given by the following equation ([Johnson et al. 1971](#)):

$$F_E = 4 \left[\left(\frac{a}{a_0} \right)^3 - \left(\frac{a}{a_0} \right)^{3/2} \right] F_c, \quad (\text{A.2})$$

where a is the contact radius, a_0 is the contact radius at equilibrium, $F_c = 3\pi\gamma R$ is the maximum force needed to separate the two particles in contact, γ is the surface energy, and $R = r_1/2$ is the reduced particle radius. At the equilibrium state, a_0 is given by

$$a_0 = \left(\frac{9\pi\gamma R^2}{\mathcal{E}^*} \right)^{1/3}, \quad (\text{A.3})$$

where \mathcal{E}^* is the reduced Young's modulus.

The contact radius is a function of the compression length between two particles in contact, δ , and vice versa:

$$\frac{\delta}{\delta_0} = 3 \left(\frac{a}{a_0} \right)^2 - 2 \left(\frac{a}{a_0} \right)^{1/2}, \quad (\text{A.4})$$

where $\delta_0 = a_0^2/(3R)$ is the equilibrium compression length at $a = a_0$. Two particles in contact separate when the compression length reaches the critical length, $\delta = -\delta_c$, where $\delta_c = (9/16)^{1/3}\delta_0$.

The viscous drag force is given by

$$F_D = \frac{2T_{\text{vis}}\mathcal{E}^*}{\nu^2} a v_{\text{rel}}, \quad (\text{A.5})$$

where ν is Poisson's ratio, v_{rel} is the normal component of the relative velocity of the two particles, and T_{vis} is the viscoelastic timescale (see [Krijt et al. 2013](#)).

In this study, we consider two cases: $T_{\text{vis}} = 0$ ps and $T_{\text{vis}} = 6$ ps. We set $T_{\text{vis}} = 6$ ps in our previous studies (e.g., [Arakawa et al. 2022a](#)), and the choice of $T_{\text{vis}} = 6$ ps is motivated by extrapolation of laboratory experiments (see Figure 5 of [Arakawa & Krijt 2021](#)). [Krijt et al. \(2013\)](#) predicted that T_{vis} would be approximately proportional to R , and [Arakawa & Krijt \(2021\)](#) confirmed this relation using experimental results of [Gundlach & Blum \(2015\)](#) and [Musiolik et al. \(2016\)](#).

The potential energy for normal motion of the two particles in contact, U_n , is given by

$$\frac{U_n}{F_c\delta_c} = 4 \times 6^{1/3} \times \left[\frac{4}{5} \left(\frac{a}{a_0} \right)^5 - \frac{4}{3} \left(\frac{a}{a_0} \right)^{7/2} + \frac{1}{3} \left(\frac{a}{a_0} \right)^2 \right]. \quad (\text{A.6})$$

The energy needed to break a contact in equilibrium by a quasistatic process (i.e., $v_{\text{rel}} \rightarrow 0$ and $F_D \rightarrow 0$), E_{break} , is

$$\begin{aligned} E_{\text{break}} &= U_n(-\delta_c) - U_n(\delta_0) \\ &= \left(\frac{4}{45} + \frac{4}{5} \times 6^{1/3} \right) F_c\delta_c, \end{aligned} \quad (\text{A.7})$$

and E_{break} is proportional to $r_1^{4/3}$.

Appendix A.2: Tangential motion

The tangential motion of two particles in contact is the combination of three motions: rolling, sliding, and twisting. The displacements corresponding to these motions are described as the rotation of two particles in contact. [Wada et al. \(2007\)](#) provided the particle interaction model for these tangential motions (see also [Dominik & Tielens 1995, 1996](#)), which is equivalent to the linear spring model with critical displacements to their elastic limits. The concept of the tangential interaction model is summarized in Figures 2 and 3 of [Wada et al. \(2007\)](#).

Appendix A.2.1: Rolling motion

The spring constant for the rolling displacement, ξ , is k_r . For the frictional model, we set

$$k_r = \frac{4F_c}{R}, \quad (\text{A.8})$$

and we set $k_r = 0$ for the frictionless model. The energy needed to rotate a particle by $\pi/2$ radian around its contact point, E_{roll} , is useful to interpret the collisional outcomes of dust aggregates from energetics (e.g., [Dominik & Tielens 1997](#)). [Wada et al. \(2007\)](#) derived that E_{roll} is given by

$$\begin{aligned} E_{\text{roll}} &= k_r \xi_{\text{crit}} \pi R \\ &= 12\pi^2 \gamma R \xi_{\text{crit}}, \end{aligned} \quad (\text{A.9})$$

where ξ_{crit} is the critical rolling displacement. In this study, we set $\xi_{\text{crit}} = 0.8$ nm for water ice particles of $r_1 = 0.1$ μm . The dependence of ξ_{crit} on r_1 is poorly understood, however (see [Arakawa et al. 2022a](#), and references therein).

Appendix A.2.2: Sliding motion

The spring constant for the sliding displacement, ζ , is k_s . For the frictional model, we set

$$k_s = 8a_0\mathcal{G}^*, \quad (\text{A.10})$$

where $\mathcal{G}^* = \mathcal{G}/[2(2-\nu)]$, and \mathcal{G} is the shear modulus. We set $k_s = 0$ for the frictionless model, as is the case for k_r . The critical sliding displacement, ζ_{crit} , is given by $\zeta_{\text{crit}} = [(2-\nu)/(16\pi)]a_0$ ([Wada et al. 2007](#)). The energy needed to slide a particle by $\pi/2$ radian around its contact point, E_{slide} , is given by

$$\begin{aligned} E_{\text{slide}} &= k_s \zeta_{\text{crit}} \pi R \\ &= \frac{1}{4} \mathcal{G} a_0^2 R, \end{aligned} \quad (\text{A.11})$$

and E_{slide} is proportional to $r_1^{7/3}$.

Appendix A.2.3: Twisting motion

The spring constant for the twisting displacement, ϕ , is k_t . For the frictional model, we set

$$k_t = \frac{16}{3} \mathcal{G}' a_0^3, \quad (\text{A.12})$$

where $\mathcal{G}' = \mathcal{G}/2$ is the reduced shear modulus. We set $k_t = 0$ for the frictionless model, as is the case for k_r and k_s . The critical angle for twisting, ϕ_{crit} , is set to $\phi_{\text{crit}} = 1/(16\pi)$ (Wada et al. 2007). The energy needed to twist over $\pi/2$ radian, E_{twist} , is given by

$$\begin{aligned} E_{\text{twist}} &= k_t \phi_{\text{crit}} \frac{\pi}{2} \\ &= \frac{1}{12} \mathcal{G} a_0^3, \end{aligned} \quad (\text{A.13})$$

and E_{twist} is proportional to r_1^2 .

Appendix B: Collisional growth efficiency

Figure B.1 shows the collisional growth efficiency, f_{gro} . The square of the normalized impact parameter ranges from $B_{\text{off}}^2 = 0$ to 1 with an interval of $1/12$. The collision velocity is set to $10^{(0.1i)} \text{ m s}^{-1}$, where $i = 10, 11, \dots, 20$. Each panel shows f_{gro} for different particle interaction models. The gray lines in Figure B.1 are the B_{off} -weighted collisional growth efficiency, $\langle f_{\text{gro}} \rangle$, and they are identical to those shown in Figure 2.

Appendix C: Energy dissipation and interparticle connection/disconnection

Here we briefly check the energy dissipation in our simulations (Appendix C.1). In addition, we also show the numbers of connection and disconnection events (Appendix C.2).

Appendix C.1: Energy dissipation

Figure C.1 shows the total energy dissipation due to particle interactions from the start to the end of the simulations, $E_{\text{dis,tot}}$ (see also Figure 8 of Arakawa et al. 2022a). For frictionless models, $E_{\text{dis,tot}}$ is given by $E_{\text{dis,tot}} = E_{\text{dis,c}} + E_{\text{dis,v}}$, where $E_{\text{dis,c}}$ is the energy dissipation due to the connection and disconnection of particles and $E_{\text{dis,v}}$ is the energy dissipation due to the viscous drag force. The gray dashed line denotes the initial kinetic energy.

The relation between $E_{\text{dis,tot}}$ and f_{gro} is complex. At approximately $v_{\text{col}} = 10 \text{ m s}^{-1}$, $E_{\text{dis,tot}}$ for frictionless models is larger than that for frictional models; however, $\langle f_{\text{gro}} \rangle$ for frictionless models is lower than that for frictional models (see Figure 2). For $B_{\text{off}}^2 = 0$ and $v_{\text{col}} = 100 \text{ m s}^{-1}$, $E_{\text{dis,tot}}$ is nearly equal to the initial kinetic energy in Figures C.1(a), C.1(b), and C.1(d), and $f_{\text{gro}} \sim 1$ in these cases (see Figure B.1). In contrast, $E_{\text{dis,tot}}$ is significantly smaller than the initial kinetic energy in Figure C.1(c), and the corresponding growth efficiency is $f_{\text{gro}} \sim -1$ in this case.

Figure C.2 shows $E_{\text{dis,c}}$ as a function of v_{rel} and B_{off} . We note that $E_{\text{dis,c}}$ is identical to $E_{\text{dis,tot}}$ for the frictionless model without normal dissipation (Figure C.2(c)). It is clear that $E_{\text{dis,c}}$ for frictionless models is larger than that for frictional models in the range of $10 \text{ m s}^{-1} \leq v_{\text{col}} \leq 100 \text{ m s}^{-1}$. For frictional models, the fraction of energy dissipation due to the connection and disconnection of particles is notably small: $E_{\text{dis,c}}/E_{\text{dis,tot}} \ll 1$. This is because the main energy dissipation mechanism for collisions of dust aggregates is the tangential friction between particles in contact for frictional models (Arakawa et al. 2022b,a).

Appendix C.2: Interparticle connection and disconnection

We also check the numbers of connection and disconnection events, as they are directly related to $E_{\text{dis,c}}$. Figures C.3 and C.4 show the numbers of connection and disconnection events in a collision between dust aggregates, N_{con} and N_{cut} , respectively (see also Figure 15 of Arakawa et al. 2022b).

For frictionless models, N_{con} is larger than N_{tot} in the range of $10 \text{ m s}^{-1} \leq v_{\text{col}} \leq 100 \text{ m s}^{-1}$ (Figures C.3(c) and C.3(d)). In contrast, N_{con} is smaller than N_{tot} for frictionless models at approximately $v_{\text{col}} = 10 \text{ m s}^{-1}$ (Figures C.3(a) and C.3(b)). The large difference in N_{con} would be related to the difference in the degree of deformation of aggregates after collisions.

For the frictionless model without normal dissipation, not only N_{con} but also N_{cut} exceeds N_{tot} in the entire range of $10 \text{ m s}^{-1} \leq v_{\text{col}} \leq 100 \text{ m s}^{-1}$ (Figure C.4(c)). For other models, N_{cut} is significantly smaller than N_{tot} at approximately $v_{\text{col}} = 10 \text{ m s}^{-1}$ (Figures C.4(a), C.4(b), and C.4(d)). As shown in Figure 2, $\langle f_{\text{gro}} \rangle$ for the frictionless model without normal dissipation is notably lower than those for the other three models. We therefore imagine that the dependence of $\langle f_{\text{gro}} \rangle$ on v_{col} might be the key to understanding the large difference in v_{fra} among particle interaction models.

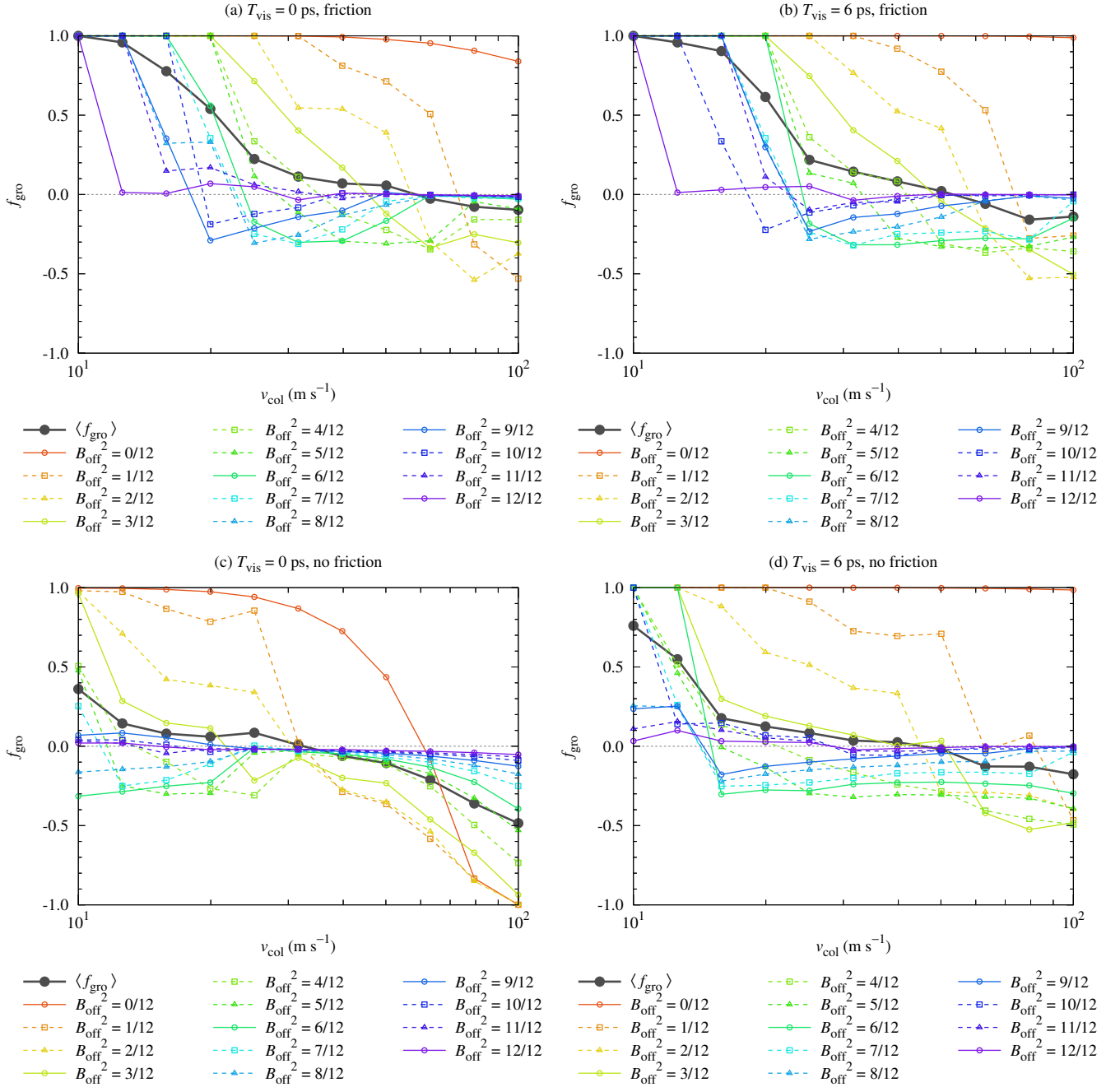


Fig. B.1. Collisional growth efficiency, f_{gro} , for different settings of B_{off} and v_{col} . (a) For the frictional model without normal dissipation. (b) For the frictional model with normal dissipation. (c) For the frictionless model without normal dissipation. (d) For the frictionless model with normal dissipation.

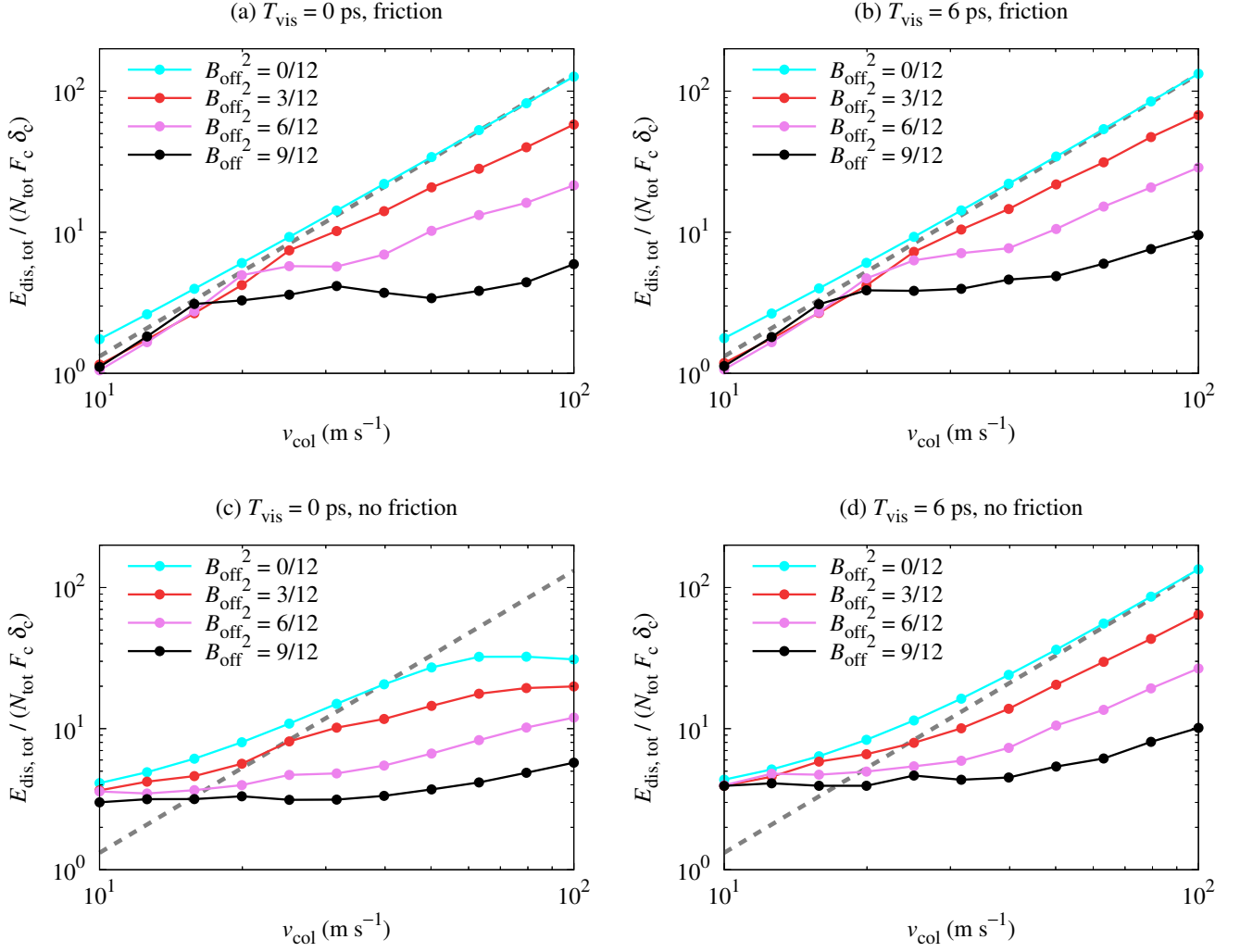


Fig. C.1. Total energy dissipation due to particle interactions from the start to the end of the simulations, $E_{\text{dis,tot}}$, as a function of v_{rel} and B_{off} . (a) For the frictional model without normal dissipation. (b) For the frictional model with normal dissipation. (c) For the frictionless model without normal dissipation. (d) For the frictionless model with normal dissipation. The gray dashed line denotes the initial kinetic energy (see [Arakawa et al. 2022a](#)).

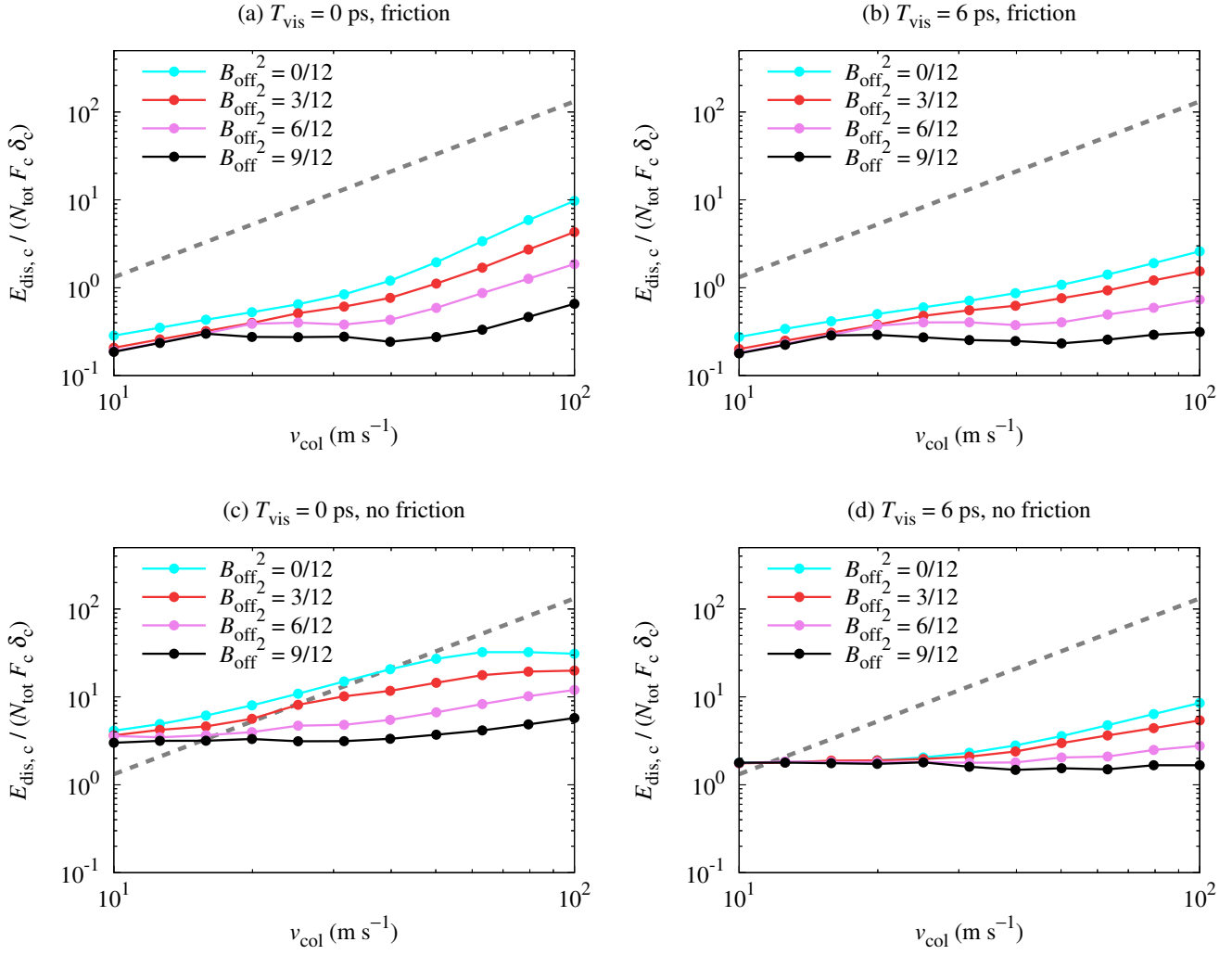


Fig. C.2. Energy dissipation due to connection and disconnection of particles, $E_{\text{dis},c}$, as a function of v_{rel} and B_{off} . (a) For the frictional model without normal dissipation. (b) For the frictional model with normal dissipation. (c) For the frictionless model without normal dissipation. (d) For the frictionless model with normal dissipation. The gray dashed line denotes the initial kinetic energy.

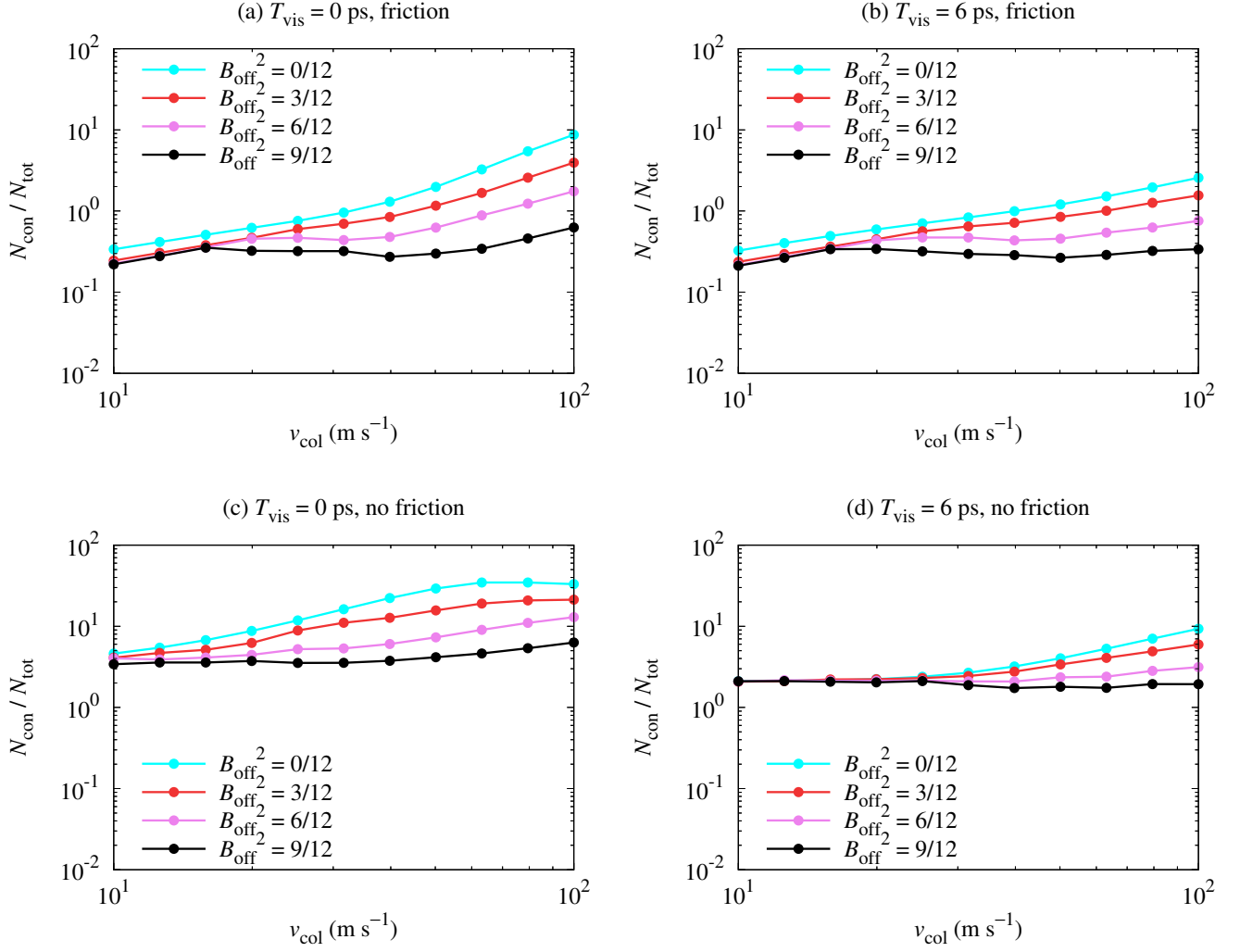


Fig. C.3. Number of connection events in a collision between dust aggregates, N_{con} , as a function of v_{rel} and B_{off} . (a) For the frictional model without normal dissipation. (b) For the frictional model with normal dissipation. (c) For the frictionless model without normal dissipation. (d) For the frictionless model with normal dissipation.

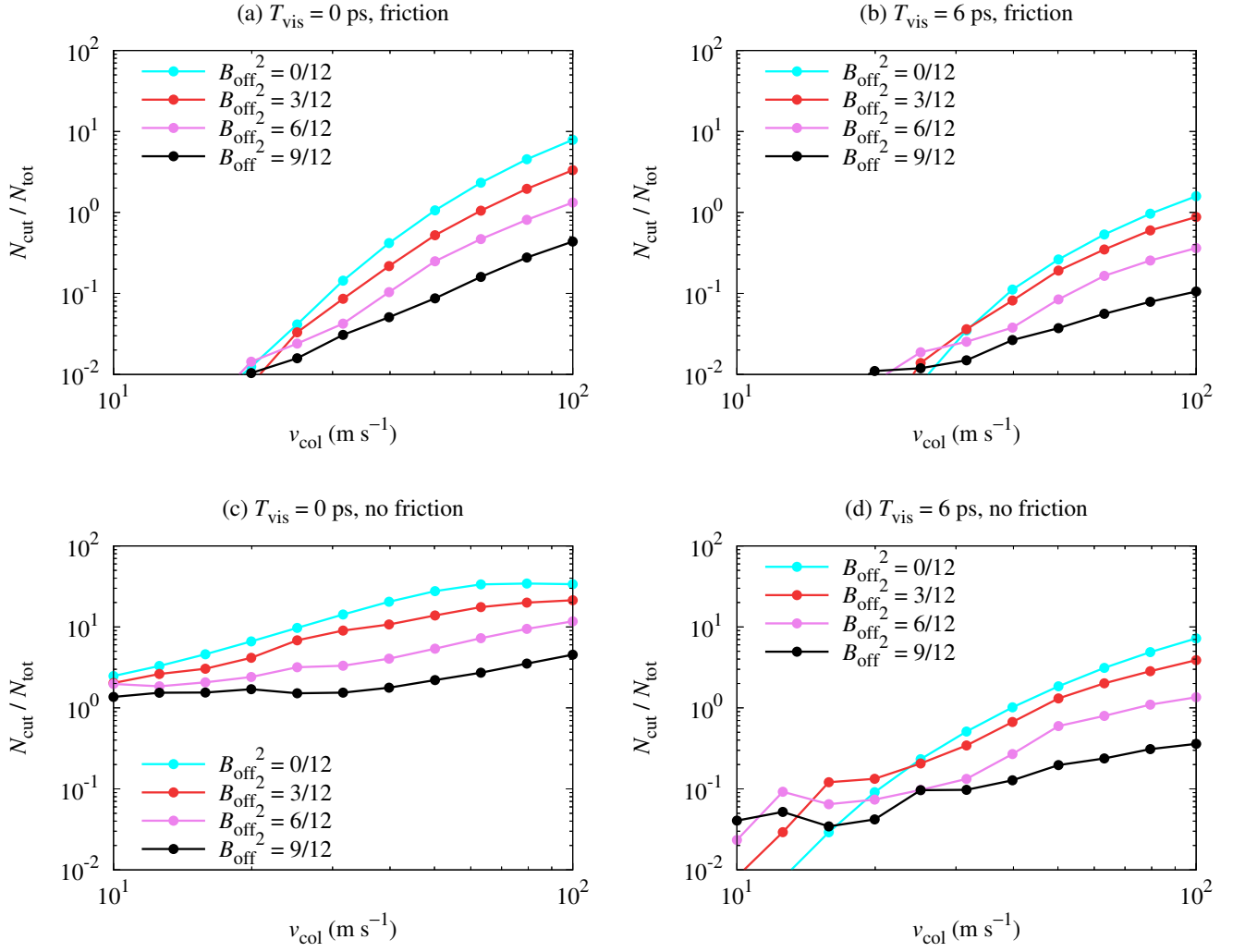


Fig. C.4. Number of disconnection events in a collision between dust aggregates, N_{cut} , as a function of v_{rel} and B_{off} . (a) For the frictional model without normal dissipation. (b) For the frictional model with normal dissipation. (c) For the frictionless model without normal dissipation. (d) For the frictionless model with normal dissipation.